Contrib Mineral Petrol
DOI 10.1007/s00410-011-0656-x

ORIGINAL PAPER

Distribution of brine in grain boundaries during static recrystallization in wet, synthetic halite: insight from broad ion beam sectioning and SEM observation at cryogenic temperature

Guillaume Desbois · Janos L. Urai · Peter A. Kukla · Uwe Wollenberg · Fabián Pérez-Willard · Zsolt Radó · Sandor Riholm

Received: 7 January 2011 / Accepted: 24 May 2011

Abstract We report observations from room temperature static recrystallization experiments (annealing times from minutes to year) of cold-pressed, synthetic, coarse-grained, wet sodium chloride, prepared by broad ion beam polishing and SEM observations at cryogenic temperature to observe directly the brine in grain boundaries. At all stages of annealing, the majority of the brine in the samples is connected in 2D sections along grain boundaries. Another part of the brine is in isolated brine inclusion arrays along grain boundaries and in brine inclusions left behind by migrating brine-filled grain boundaries. Most of these boundaries are mobile because the aggregate is coarsening. We interpret that the boundaries without observable brine films (< 15 nm) and brine inclusion arrays are healed and immobile. Evolution of grain boundary structure involves three major processes. First, dissolution on one side of the grain boundary and precipitation on the other side, resulting in grain boundary migration. Second, the development of facets formed by low-index crystallographic planes of the grains bounding the grain boundary brine. When both sides of a grain boundary are able to develop low-index facets in a thick brine film, the resulting impingement boundary is interpreted to be immobile and may prevent the new grain from migrating into a deformed neighbor. When one side of a faceted boundary consists of low-index crystallographic planes and the other side passively follows this faceted shape along irrational surfaces, the boundary is mobile. Third, the healing of grain boundary brine films, producing solid–solid grain boundaries without resolvable brine films.

Communicated by J. Hoefs.

Electronic supplementary material The online version of this article (doi:10.1007/s00410-011-0656-x) contains supplementary material, which is available to authorized users.

G. Desbois (&) · J. L. Urai
Structural Geology, Tectonics and Geomechanics,
RWTH Aachen University, Lochnerstrasse 4-20,
52056 Aachen, Germany
e-mail: g.desbois@ged.rwth-aachen.de

P. A. Kukla · U. Wollenberg
Geological Institute, RWTH Aachen University, Wüllnerstr. 2,
52062 Aachen, Germany

F. Pérez-Willard
Carl Zeiss NTS GmbH, Carl-Zeiss Str. 56,
73447 Oberkochen, Germany

Z. Radó · S. Riholm
Technoorg-Linda Ltd.Co, Keve Utca 24,
1077 Budapest, Hungary

Published online: 15 June 2011

Keywords Static recrystallization · Halite · BIB-cryo-SEM · Brine-filled GB · In situ GB microstructures

Introduction

The presence of brine in halite strongly affects its mechanical and transport properties (Urai et al. 2008). Solution-transfer creep and dynamic recrystallization are dramatically enhanced by the presence of brine at grain boundary, with major changes in rheology. In addition, rock salt forms seals for hydrocarbon accumulations, aquitards, and chemical barriers. Therefore, a detailed knowledge of grain boundary microstructures in wet halite is fundamental for modelling and prediction of deformation and transport in a wide range of geological environments (Hudec and Jackson 2007; Schoenherr et al. 2007; Desbois et al. 2010) as well as for the storage of gas, anthropogenic carbon dioxide, and radioactive waste (Pinc 1985;

Staudtmeister and Rokahr 1997; Langer 1993; Berest et al. 2010) in deep geologic formations.

In evaporite minerals, the structure of mobile brine-filled grain boundaries and their influence on recrystallization processes were intensively investigated in theoretical and experimental studies (Urai et al. 1986b; Brantley et al. 1990; Drury and Urai 1990; Hickman and Evans 1991, 1995; Gratier 1993; Heidug and Leroy 1994; Lehner 1995; Holness and Lewis 1997; Spiers and Schutjens 1999; Visser 1999; Ghoussoub and Leroy 2001; De Meer et al. 2002, 2005; Den Brok et al. 2002; Watanabe and Peach 2002; Lohkaemper et al. 2003; Renard et al. 2004; Schenk and Urai 2004, 2005; Van Noort et al. 2006, 2008).

However, interpretation of results from these studies is still a matter of debate because of the difficulty to observe the morphology of in situ wet grain boundaries at a resolution of nanometers (De Meer et al. 2005; Desbois et al. 2008). One recently explored method is to rapidly freeze the samples to very low temperatures, which effectively quenches the brine-filled grain boundaries without crystallization of the brine, followed by high-resolution electron microscopy at cryostatic temperatures (Schenk et al. 2006; Holzer et al. 2007, 2010; Desbois et al. 2008, 2009). Cryo-SEM can be combined with a Focussed Ion Beam (FIB) milling to prepare smooth, damage-free surfaces (Holzer et al. 2007, 2010; Desbois et al. 2008, 2009; Holzer and Cantoni 2011). Commercial FIB tools in SEM are based on Gallium ion sources (1 pA to 50 nA) to produce typical cross-sections of a few μm^2, with serial sectioning for the investigation of microstructures in 3D (Holzer et al. 2007, 2010; Desbois et al. 2008; De Winter et al. 2009). Broad ion beam (BIB; up to few mA, argon source) cross-sectioners are commercially available as stand-alone machines, to produce polished cross-sections at room temperature of much larger area than the FIB. Because the BIB source is not focused, a shielding plate is placed on the top surface of the sample in order to create a flat cross-section. BIB has two main advantages: (1) it is potentially less damaging since it is based on noble gas source and (2) it is able to produce polished surfaces up to few mm^2, about hundred times bigger than those produced by FIB. This last feature is of particular interest for geomaterials since it fits better to the typical length scale range of microstructures and representative elementary area.

Schenk and Urai (2004), studied wet, coarse-grained (200–355 μm), compacted samples of synthetic sodium chloride which undergo recrystallization and grain growth at room temperature to produce large (up to 3000) strain-free grains growing into deformed old grains. The new grains are frequently euhedral with mobile grain boundaries moving at time-averaged velocities up to 6 nm/s. Arguments in favor of the existence of brine-enriched zones on grain boundaries were the following: (1) the efflorescence from such boundaries upon drying, (2) euhedral shape of the growing grains, and (3) the high migration rates. However, details of the brine distribution and its influence on grain boundary migration were only partly resolved, because brine was removed during sample preparation. In a later study, Schenk et al. (2006) studied brine-filled grain boundaries in similar coarse-grained samples by cryo-SEM on freeze-fractured surfaces. They found evidence for brine at the boundaries of the primary recrystallizing grains indicating the existence of brine films with a thickness between a few μm and 30 nm. In this last study, the observation of brine-filled grain boundaries was difficult because of the surface roughness induced by fracturing the sample during preparation. The process of brine-assisted grain boundary migration was interpreted to occur simultaneously with surface energy-driven grain boundary healing, which dramatically reduces grain boundary mobility (Hickman and Evans 1991; Lehner 1995; Visser 1999; Ghoussoub and Leroy 2001; Schenk and Urai 2004, 2005; Schléder and Urai 2005; Van Noort et al. 2008).

This contribution reports of experiments that were identical to Schenk and Urai (2004) and Schenk et al. (2006) to study the distribution of brine in moving grain boundaries during static recrystalization in synthetic, coarse-grained wet sodium chloride, annealed at room temperature over periods between a few minutes and 1 year. Here, we used a novel and unique BIB-cryo-SEM instrument combining in situ broad ion beam (BIB) cross-sectioning and state-of-the-art SEM cryo-SEM to study brine into grain boundary.

The BIB-cryo-SEM instrument

The BIB-cryo-SEM instrument used in this contribution combines a state-of-the-art field emission SEM for high-resolution imaging (SE and BSE detectors, EDX system), with an argon broad ion beam excavation system and a cryogenic workstation (shock-freezing stage, cryo-preparation chamber with cold knife and coating system). A detailed description of all facilities included in this instrument as installed at RWTH Aachen University (Germany) is given in Online Resource 1.

After freezing the samples and inserting into the cryo-SEM, (Fig. 1), the shielding plate is positioned onto the sample surface in the region of interest by nanomotor positioning. The BIB is placed at 70° from the electron beam. In condition of milling, the BIB, with beam diameter around 800 μm in size, irradiates both the region of interest in the sample and the edge of the mask designed with a slope of 20. One half of the BIB is masked by the shielding plate, and the part of the beam, which is not

Table 1 Overview of samples investigated in this contribution

Sample	Number of samples	Starting grain size (μm)	Annealing time[a]
20 min	2	200–355	18 min
			15 min
2 h	2	200–355	1 h, 54 min
			1 h, 56 min
2 days	2	200–355	2 days, 2 h, 7 min
			1 day, 23 h, 46 min
1 week	2	200–355	5 days, 22 h, 30 min
			6 days, 23 h, 6 min
2 weeks	2	200–355	14 days, 19 h, 10 min
			14 days, 15 min
1 month	2	200–355	24 days, 19 h, 20 min
			30 days, 18 h, 8 min
1 year	3	200–355	1 year–1 year, 2 months

[a] The annealing was carried out at room temperature

Fig. 1 Principle of in situ BIB milling into the SEM. The original wet sample is first vitrified in slushy nitrogen using the cryo-unit and then transferred inside the SEM by the cryo-preparation chamber. Once the sample is placed on the SEM sample stage, a titanium blade is positioned over the region of interest using a 3 axis Cartesian nanomotor. The argon ion beam irradiates both the region of interest in the sample and the edge of the mask designed with a slope of 20°. Beneath the edge of blade, the density of ions is maximal and the split beam is parallel to the blade edge. This configuration allows creating a vertical 2D cross-section directly beneath the titanium blade suitable for imaging microstructures at SEM resolution (e-beam)

masked, excavates the sample producing a cross-section. After milling, the cross-section is suitable for SEM investigations.

Samples and sample preparation

Samples are compacted synthetic polycrystals from commercial halite powder (NaCl content [99.9%) prepared as in Schenk and Urai (2004). After treating for 30 s in an ultrasonic bath, the initial salt/brine mixture (grain size in the range of 200–355 μm) was poured into the cylindrical die of a uniaxial compaction apparatus. Subsequently, the pressure on the upper piston was raised to 150 MPa in a few minutes and maintained for 5 min. Resulting samples are dense cylindrical disks with a diameter of 1 cm and a height of 1–1.5 mm. Produced samples were then annealed (from about 20 min. to more than 1 year, see Table 1) in salt/brine-saturated atmosphere in order to allow static recrystallization of samples (Schenk and Urai 2004).

BIB-cryo-SEM experiments were performed on 15 different samples (Table 1) following the same procedure of sample preparation and imaging: (a) the in situ wet sample is mounted on the appropriate sample holder at room temperature; (b) plunged frozen in slushy nitrogen, stirring to minimize the Leidenfrost effect (Desbois et al. 2008); (c) via the cryo shuttle operating at cryogenic temperatures and vacuum conditions, the sample is transferred from the slushy nitrogen container to the cryo-preparation chamber; (d) the surface of sample is coated with platinum (15 A, 50 s.) at cryo-temperature; (e) transfer from the cryo-preparation chamber to the SEM sample stage maintained at cryo-temperature via the same cryo shuttle previously mentioned; (f) the cross-section is then cut at cryo-temperature, on frozen/stabilized samples using the BIB gun for 3 h at 8 kV acceleration voltage; (g) when cross-section is complete, SEM imaging is typically performed at 3 kV for a working distance of around 16 mm and aperture of 30 μm, on non-coated cross-section.

To reveal the crystal orientation patterns, the EBSD analysis (Electron Back Scattered Diffraction) on JEOL JSM 7000F SEM (Gemeinschaftslabor fuer Elektronenmikroskopie, RWTH Aachen) with EDAX-TSL DigiView III detector equipped with OIM Data Collection/OIM Analysis (version 5.2) software was employed. The patterns were acquired at acceleration voltage of 25 kV, probe current ~15 nA, and working distance 29 mm. Several regions of interest from BIB section of a sample annealed for 4 days were scanned in an area of about 300 × 300 μm at a magnification of 750× with and step size of 0.25 microns. Because EBSD tool is not available in BIB-cryo-SEM machine, EBSD analysis was performed on sample dried at 80C for 3 days.

Results

Cross-section overviews and surface quality

Figure 2 presents typical cross-sections obtained at 8 and 10 kV (BIB acceleration voltage) under cryogenic conditions. All samples were cut in a plane, which contains the

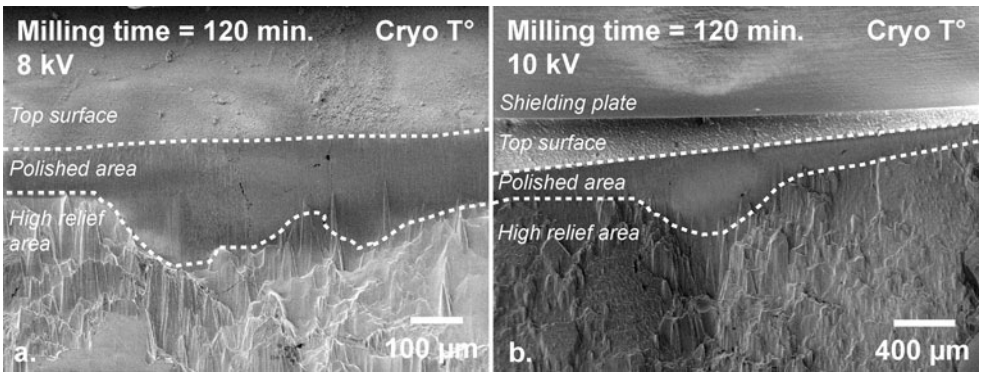

Fig. 2 Overview of typical cross-sections produced by in situ BIB milling (120 min) into the SEM at cryo-temperature at acceleration voltage of 8 kV (a) and 10 kV (b). Cross-sections have a typical pseudo-Gaussian shape reßecting the ion density in the beam. High relief areas correspond to material regions being removed

direction of compression. Resulting cross-sections have pseudo-Gaussian shape reßecting the ion density distribution in the beam split by the shielding plate and the typical high relief in the areas being removed. For NaCl, milling rates of about 350 µm/hr at 10 kV, 150 µm/hr at 8 kV, and 60 µm/hr at 6 kV are typical values.

The quality of cross-sections is reproducible. At the scale of ÔÔoverviewÕÕ (Fig. 2), cross-sections appear ßat; at higher magniÞcations (Figs. 4, 5, 7 and Online Resource 2), surfaces show curtaining parallel to the beam direction with a regular wavelength in the range of 1–2 µm and a topography in the range of few nanometers. In ßat section of the ÔÔcurtainsÕÕ, microstructures down to 15 nm are resolved.

In previous contributions dealing with cryo-SEM on wet rock salt (Schenk et al. 2006; Desbois et al. 2008), in situ brines were sublimated to help with the detection of brine distribution. This technique is also called freeze-drying. Freeze-dried brine has a characteristic foam-like morphology (Schenk et al. 2006; Desbois et al. 2008), which can be used to decorate and thus detect brine. In this contribution, brine also develops a foam texture (Figs. 5, 7 and Online Resource 2).

Interface nomenclature

To facilitate the description of grain boundaries, we propose to introduce the following nomenclature (Fig. 3). The HH boundary is a boundary between two halite grains, with no visible structure at the scale of observation. This means that at low magniÞcation, boundaries, which can be shown to contain a brine Þlm, are called HH. The HBH boundary, where there is resolvable brine between two halite grains at the scale of observation. The HÐB boundary is the contact between halite and brine. Therefore, a brine-Þlled boundary consists of two HB boundaries (HB BH=HBH)

Fig. 3 Interface nomenclature. The HBH boundary is a interface with resolvable brine between two halite grains, and HH boundary is a boundary between two halite grains, with no visible structure, both at the scale of observation. In case of HBH boundary, the shape of the boundaries can be faceted (*straight*, indicated by subscript f) or non-faceted (*curved*, subscript n)

The shape of the boundaries can be faceted (straight, indicated by subscript f) or non-faceted (curved, subscript n). Again, this is deÞned at the relevant scale of observation.

Thus, a boundary with resolvable brine, which is faceted on one side and curved on the other side of the brine Þlm, is called a HBH_n boundary. The same structure at much lower magniÞcation is called a HH boundary (Fig. 4).

Grain microstructures

At the scale of a few micron, in the whole sample, (Fig. 5a, b, and B.1 in Online Resource 2), halite grains up to 0.1 mm in size with serrated HBH_n boundaries containing up to 1 µm thick brine Þlms are common. The shape of these grains varies from elongated to equiaxed (Fig. 5a and B.1 in Online Resource 2).

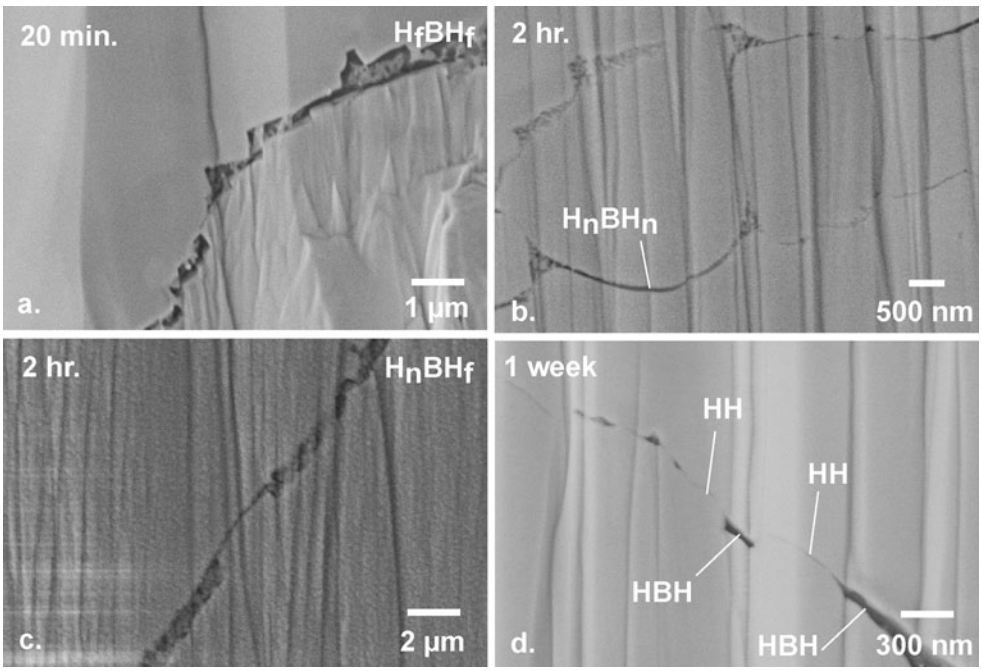

Fig. 4 SE micrographs of different halite–brine interfaces detected in samples. a H_fBH_f b H_nBH_n boundary with low wavelength curved HB interfaces. c H_nBH_f d HH and HBH boundaries at high magnification. Interfaces are described by the following abbreviations: H halite, B brine, n non-faceted f faceted (see also Fig. 3)

Estimates of the total amount of brine in the samples using our images are in agreement with the brine-filled porosities measured (~2.5%) by Schenk and Urai (2004).

Between large grains, there are small euhedral single grains with rounded corners up to 150 µm in size (core mantle microstructure, Figs. 5c, d, 6 and B.2 in Online Resource 2). In 2D sections, these crystals are surrounded by brine and sometimes occupy the majority of the zone between the boundaries of the large grains (Fig. 6 and B.2.c in Online Resource 2). These small euhedral grains were absent in samples annealed for more than a few weeks.

A second class of grains bounded by facets is defined by a larger grain size (> 2 µm) and more complex facet structures (Fig. 5e, f, and B.3 in Online Resource 2). These euhedral grains have multiple facets defining morphologies from flat (Fig. 5e and B.3.a, b, c, e, f in Online Resource 2) to round (Fig. 5f and B.3.a, c, f in Online Resource 2) and step-shaped (Figure B.3.d in Online Resource 2).

Brine distribution

At higher magnification (below one micron, Fig. 7), brine-filled grain boundaries show strong variations in the morphology of the halite–brine contacts. We observed all possible types H_fBH_n, H_fBH_f, H_nBH_n, and HH (Fig. 4). Thus, one side of the brine film can have a faceted morphology while the other side is wavy. Independently of annealing time, brine filled all space between halite grains (there was no evidence for gas inclusions in the brine).

For all annealing times, continuous brine-filled grain boundaries are frequent, with variable thickness from about 15 nm (limit of resolution) to more than 1 µm (Figs. 4, 5, 7d and Online Resource 2) over long sections (up to few hundreds micrometers). The thickest brine-filled continuous grain boundaries (> 1 µm) bound the largest grains with H_nB contacts (Figs. 5a, b, 7g and B.1 in Online Resource 2), while brine films with thicknesses below 1 µm are usually at interfaces involving at least one H_fBH contact (Fig. 5e, f, and B.3 in Online Resource 2). Exceptions are curved H_nBH_n boundaries with high wavelength (Fig. 4b and B.3.f in Online Resource 2) with typical brine film thickness < 50 nm.

Irregular brine pockets between grains are bound by H_fBH_f boundaries. The geometry of boundary impingement controls the morphologies and area (up to few µm^2) of these irregular brine pockets (Fig. 5e, f, and B.3 in Online Resource 2). Adjacent irregular brine pockets can be connected by very small brine-filled throats down to 15 nm thick controlled by facets developed by the host grains (Fig. 5e, f and B.3 in Online Resource 2).

In contrast to irregular brine pockets, there are intergranular brines inclusions (IBI, size smaller than 500 nm) in HH–HH grain boundaries, which are not defined by H_fBH_f

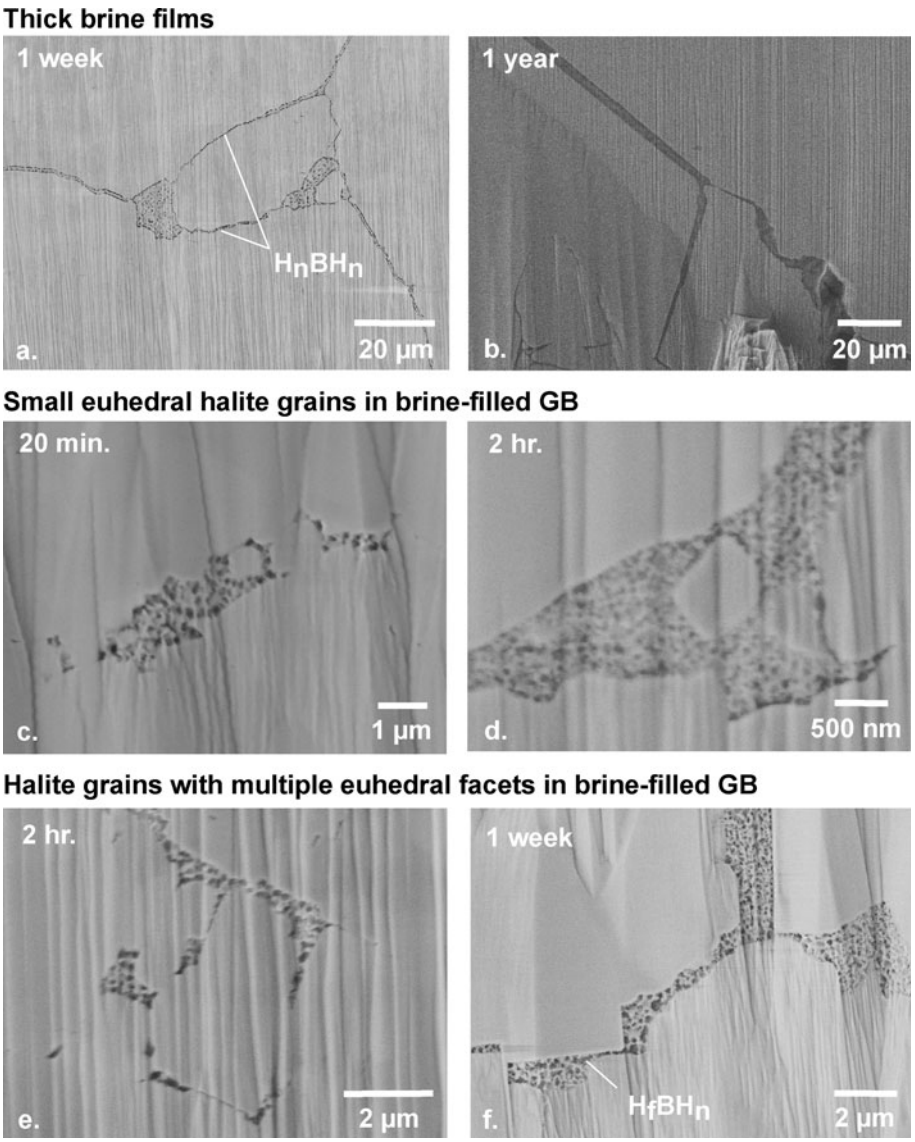

Fig. 5 SE micrographs of grain boundaries interfaces taken at different annealing times. a and b depict networks of thick brine films (> 1 µm). c and d show small euhedral halite grains which appear floating in brine-filled grain boundaries identified in Fig. 4. These small new grains are frequent for short annealing times. e and f show halite grains with multiple euhedral edges. These grains are slightly bigger than those presented in c and d and exhibit more complex face structures according to the Hartman–Perdok theory for cubic crystals. Interfaces are described by the following abbreviations: *H* halite, *B* brine, *n* non-faceted, *f* faceted (see also Fig. 3). For additional pictures, please check also the Online Resource 2

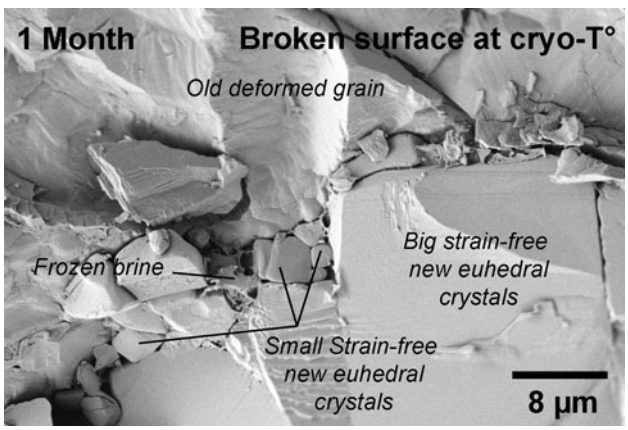

Fig. 6 SE micrograph of a freeze-fractured broken sample annealed for 1 month. This micrograph depicts a contact between a big strain-free new euhedral crystal growing toward a old deformed grain. Small strain-free euhedral crystals are also present into the grain boundary

boundaries (Fig. 7). These have three main different characteristic morphologies as follows: (i) ÔÔelongated-shapedÕÕ IBI have a very high aspect ratio with rounded (Fig. 7a) or sharp tips (Fig. 7b); (ii) ÔÔTriangle-shapedÕÕ IBI have also a high aspect ratio (Fig. 7c, d); and (iii) sub-micron arrays of ÔÔquadrangle-shapedÕÕ IBI (Fig. 7e, f). Sometimes, a very thin line (< 20 nm thick) is resolvable connecting the arrays of IBI (Fig. 7a–f). Unfortunately, since the thickness of this very thin line is in the range of the SEM resolution, it is not clear whether this is brine filled.

In addition to the first three types, there is an additional fourth type: the intragranular ÔÔquadrangle-shapedÕÕ brine inclusion (Fig. 7g). This last type differs from others because they are significantly bigger (> 1 µm in size), are not aligned with other similar IBI, and are never linked to visible ÔÔvery thin lineÕÕ as described previously.

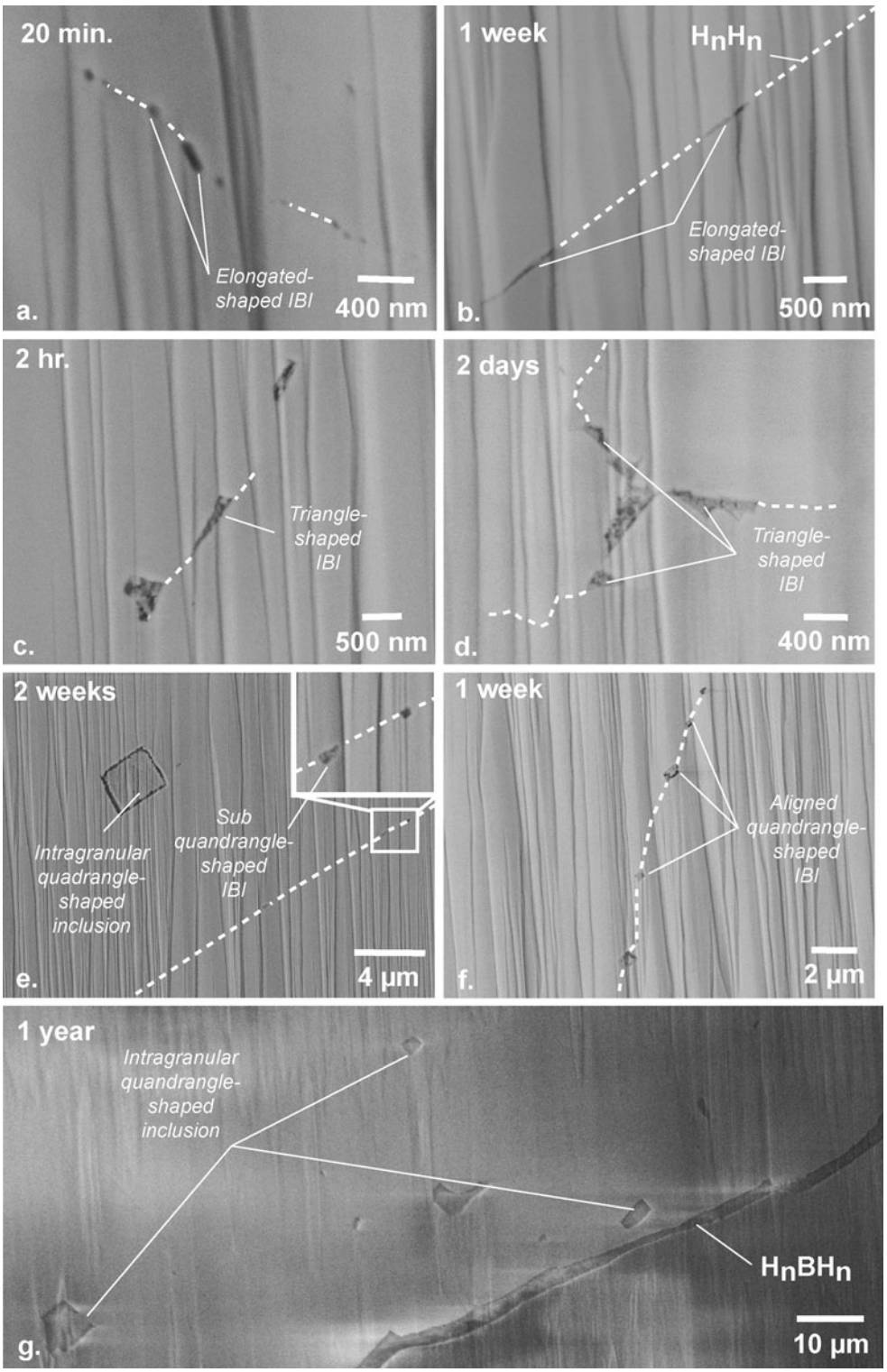

Fig. 7 SE micrographs of brine-Þlled isolated brines inclusions (IBI; \ 500 nm in size) with different characteristic morphologies and taken at different annealing times. **a** and **b** are the "*elongated-shaped*" IBI, **c** and **d** are the "*triangle-shaped*" IBI, **e** and **f** are the aligned "*quadrangle-shaped*" IBI. These IBI are interpreted to develop during grain boundary healing. All of these IBI are interpreted to reßect the end stage of brine distributions at migrating grain boundary whose different morphologies are controlled by the relative crystallographic orientation of grains at contact. The intragranular big "quadrangle-shaped" IBI (n size) are also identiÞed (**e** and **g**) and are interpreted as IBI left over migrating grain boundary. *White-dashed lines* indicate HÐH interfaces. Interfaces are described by the following abbreviations: *H* halite, *B* brine, *n* non-faceted *f* faceted (see also Fig. 3)

Each of the four different IBI described above is present in all investigated samples independently of the annealing time but intragranular ÔÔquadrangle-shapedÕÕ brine inclusions are particularly abundant in samples annealed for years.

Discussion

Quality of milled surfaces

In his current state, our BIB-cryo-SEM does not produce comparable quality surfaces to those of commercial stand-alone BIB cross-sectioners (Desbois et al. 2009; Loucks et al. 2009), since cross-sectioned surfaces presented here exhibit curtaining which can mask and distort the very small microstructures (<15 nm). The curtaining effect is known to be due to heterogeneous milling rate, driven by heterogeneities in the material. In commercial stand-alone BIB cross-sectioners, this is minimized by rocking the sample during milling along the axis perpendicular to the plane to be polished and milling at different angles. Sample rocking during milling at room temperature was recently implemented in our system. Preliminary runs produced perfect cross-sectioned surfaces without curtaining (Fig. 8). In the near future, sample rocking will be also implemented under cryogenic conditions. However, considering the limitations just discussed, many of the relevant grain boundary structures could be resolved in the development stage of the machine when sample rocking was not available, either at a scale much larger than the characteristic curtain diameter or at a scale smaller than the characteristic curtain diameter. Moreover, even in its actual state, the BIB-cryo-SEM instrument provides a better insight into pores, interfaces, and ßuid-related microstructures than previous experiments performed on similar broken samples (Schenk et al. 2006) since produced 2D cross-sections optimize the microstructural interpretations, which are difÞcult to reach when the topographies of surfaces are rough (of few ten micrometers in size for the case of broken samples). In addition, and more importantly, the BIB cut avoids the preferential exposure of parts of the microstructure when the fracture process develops along the weal parts of the sample. So, in Schenk et al. (2006), we saw only those parts of the grain boundary network, which could be exposed by fracturing. Besides this, the area size (few mm^2) of cross-sections provided by the use of BIB embedded in cryo-SEM machine allows studies in representative area.

Because samples were not freeze-dried during preparation, it is obvious that the BIB locally heats the sample during milling since frozen brine exhibits the characteristic foam pattern typical of freeze-drying (Schenk et al. 2006; Desbois et al. 2008). Freeze-dried brine during FIB milling was also observed in Desbois et al. (2008). In the future, heating of the frozen sample during BIB milling will be minimized, by lowering the current density, optimizing the distance between the shielding plate, and by cooling the mask. However, in case of wet rock salt, freeze-drying of brine is also a useful indicator for in situ brine (Schenk et al. 2006; Desbois et al. 2008).

Development of euhedral facets

Along the original grain margins (up to few hundreds micrometers in size), grains with multiple, flat facets are present (Fig. 4a, c, 5e, f, 8, and B.3 in Online Resource 2). As discussed in Schenk and Urai (2004), the origin of such faceting is due to the deformation of original halite powder in uniaxial compaction apparatus (see section ÔSamples and sample preparationÕ), which produced gradients of defect density and microcracks favorable to nucleation of

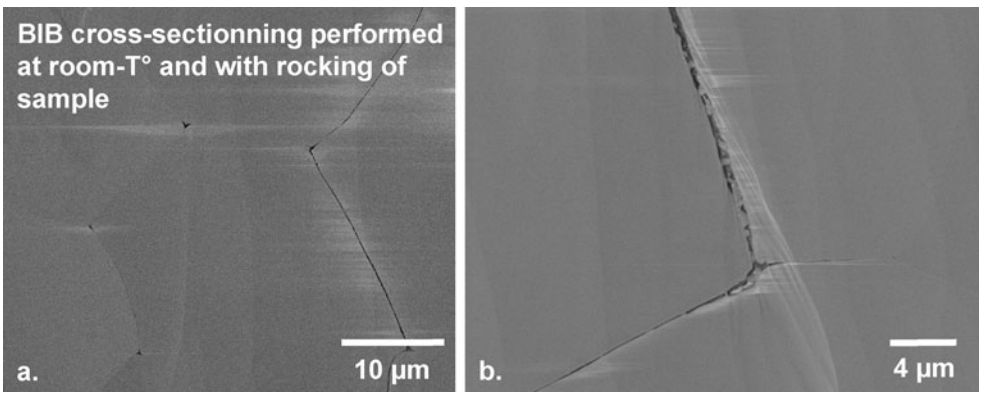

Fig. 8 SE micrographs of surfaces produced by in situ-SEM BIB cross-sectioning at room temperature with sample rotating (along axis perpendicular to the ion beam) during milling. This hardware improvement allows creating perfect surfaces without curtaining. a Grain boundary network exhibiting small triple junctions. b A grain boundary at euhedral grain edge is Þlled with halite recrystallized by rapid opening of brine-Þlled pore during BIB cross-sectioning under vacuum. Surfaces are smooth and ßat surface without critical curtaining

Fig. 9 a SEM (BSE) and b EBSD micrographs of the same local grain fabric in dried sample annealed for 4 days. Micrographs show faceted new crystals with low-index facets (euhedral growth) and free of lattice distortion. In contrast, in a.1 and a.2, the grain at right side is lattice distortion-rich pointing to old deformed grain. At the scale of observations, the numbers 1, 2, and 3 in circles indicate H_fH_{fr}, H_nH_n, and H_fBH_f interfaces, respectively. H_fH_{fr} interfaces reßect the growing of new grains at the expense of old deformed grain forming an irrational grain boundary, H_nH_n interfaces are interpreted as healed contact between two new crystals, and H_fBH_f interfaces as euhedral facets growing into ßuid-Þlled pore space. *White cube* exhibits show three-dimensinal representation of the crystallography of the respective grain showing the dominance of grain boundaries compatible with equivalent {001} facets. Interfaces are described by the following abbreviations: *H* halite, *B* brine, *n* non-faceted, *f* faceted, *i* irrational, *r* rational (see also Fig. 3 and section "Mobility of grain boundaries")

strain-free grains with H_fBH_f boundaries (Humphreys and Hatherly 1996). Such newly nucleated crystals initially develop crystal faces because they grow in a brine environment (as described by Hippert and Egydio-Silva (1996) in quartz mylonite). Due to differences in dislocation density, some old grains are interpreted to have a slightly higher solubility, providing the material for growth of the H_fB facets elsewhere. This may explain why some original grains do not exhibit faceting (Figs. 4c, 5a, b, 7g, and B.1 in Online Resource 2).

Because they are fully surrounded by brine, the small euhedral grains in the core and mantle structures (Figs. 5c, d, 6 and B.2 in Online Resource 2) are interpreted to have grown epitaxially from very Þne grains electrostatically stuck on starting material (and thus not removed by sieving) or from small grain fragments formed during cataclasis of the starting material.

Euhedral new grains exhibit multiple facets (Figs. 5e, f and B.3 in Online Resource 2) whose structure was shown to correspond to the Hartman–Perdok theory for ßat (F) faces (Hartman and Perdok 1955; Urai et al. 1986a; Van Noort et al. 2006; Schenk et al. 2006). Considering three periodic bond chains (PBC), three different types of face can be identiÞed by F, S, and K indicating a ßat face (parallel to at least two PBCÕs), a stepped face (parallel to one PBC), and a kinked face (not parallel to any PBCÕs), respectively. Our conclusions are in agreement with EBSD-based analysis of euhedral crystals in these samples (Fig. 9 and e.g. Schenk et al. 2006).

Evolution of brine-Þlled grain boundaries

At all stages of annealing, HBH boundaries are systematically brine Þlled with no evidence of gas inclusions in

brine, confirming that samples were brine saturated throughout the experiment.

The majority of brine is connected in 2D sections along grain boundaries from 15 nm up to few micrometers thick (Figs. 4, 5a, b and B.1 in Online Resource 2). This is consistent with earlier observations in experiments (Schenk et al. 2006), but in current models of equilibrated grain boundaries in natural domal salt continuous brine films are much less frequent (Spiers et al. 1986; Urai et al. 1986a). Further work is needed to resolve this discrepancy, which is of special importance for problems of nuclear waste storage in domal salt, since continuous brine-filled grain boundary networks can decrease dramatically the flow stress and sealing performance of rock salt (Littke et al. 2008). Another part of the brine is present in irregular brine pockets bounded by facets (Fig. 5e, f, and B.3 in Online Resource 2), intergranular arrays of IBI, and intragranular "quadrangle-shaped" brine inclusions (Fig. 7).

In our interpretation, the formation of HH boundaries (no brine is visible at nm-resolution) is intimately linked to the growing of new euhedral crystals (Figs. 4d, 5e, f, and B.3 in Online Resource 2). The development of facets according to the Hartman–Perdok theory closes progressively continuous HBH boundaries and irregular brine-filled pockets by the healing of the boundaries as described by Urai et al. (1986b), Spiers et al. (1990), Hickman and Evans (1991). The three different types of IBI (elongated shaped, triangle shaped, and quadrangle shaped, 1–10 μm in size; Fig. 7) are interpreted as very late stage of grain boundary healing. In majority, these IBI are not connected to each other at the ultimate resolution of the SEM (i.e., above 15 nm). However, sometimes "thin lines" are present in the queue of these inclusions (Fig. 7i), interpreted as HH boundaries. At this resolution, it is not possible to distinguish true solid–solid boundaries from a HBH boundary with a 1 nm thick brine film.

Intragranular "quadrangle-shaped" brine inclusions (Fig. 7e, g) are much larger (typical few micrometers in size) than the three IBI discussed earlier, are poorly aligned, and no H–H boundaries are visible at the immediate vicinity, suggesting that these are leftover brine inclusions behind migrating grain boundary. The frequency of these intragranular "quadrangle-shaped" brine inclusions is relatively high at long-term annealing since samples have completed their static recrystallization (Schenk and Urai 2004; Schmatz et al. 2010).

As in Fujiwara et al. (2009) for growing Si crystals, the variation of IBI morphologies address to the control of crystallographic orientations in grain impingement. Following on the arguments of Van Noort et al. (2006), the systematics of Hartman–Perdok theory is used to interpret that: (i) "elongated-shaped" IBI and intragranular "quadrangle-shaped" brine inclusions originate from the convergence of two F faces; (ii) "quadrangle-shaped" IBI reflect the contact of a S or K face with an other S or K face; and (3) "triangle-shaped" IBI correspond to the convergence of one F face with one S or K face. Previous contributions (Hickman and Evans 1991, 1995; De Meer et al. 2005; Van Noort et al. 2006) based on studies of post-mortem roughness of pressure dissolved surfaces (grain to grain indenter deforming under pressure solution) in halite–glass, halite–halite, or halite–fluorite contact systems also infer the strong influence of crystallographic orientation on the morphology of contacts and thickness of brines at grain boundaries.

Mobility of grain boundaries

Because the aggregate is coarsening (Schenk and Urai 2004), most of grain boundaries studied in this work are mobile. Unfortunately, at this point, it is not possible to directly confirm that a given boundary was moving at the moment that it was quenched for BIB-cryo sectioning.

H_fBH_n boundaries (Figs. 4c, 5f) are interpreted to be migrating boundaries, i.e., the growth of new grains at the expense of old grains driven by reduction of dislocation density in deformed grains (Fig. 9, Schenk and Urai 2004; Humphreys and Hatherly 1996).

An H_f boundary is defined in this work as a faceted boundary corresponding to low-index facets (i.e., euhedral growth, Fig. 9). Let us now introduce a second subscript (r, i) to indicate rational (low index) or irrational facets. Then, there are H_{ff} and H_{fi} boundaries. In Schenk et al. (2006) and confirmed in Fig. 9, it was shown by EBSD that euhedral new grains growing into old grains have a $_{ff}BH_{fi}$ boundary.

H_nBH_n boundaries with high wavelength (Fig. 4b and B.3.f in Online Resource 2) are interpreted to be mobile and migrating by dissolution on one side of the grain boundary and precipitation on the other side, probably because the face that is growing is strongly misoriented from F faces.

At contrary, intergranular arrays of IBI point to grain boundary healing (Fig. 7). Grain boundary healing is assumed to be responsible for $_nHH_n$ interfaces (If a thin brine film really exists, it is less than 15 nm thick, i.e., below the resolution of the SEM), and it is interpreted to form the end stage of brine redistribution during static recrystallization and the end of grain boundary migration. Therefore, intergranular arrays of IBI with a variety of shapes related to the orientation of host grains are considered as immobile. Since the first IBI appear after around few 10 min (Fig. 7a), under favorable conditions grain boundary healing locally can be a very fast process in our experiments (Schenk and Urai 2004; De Meer et al. 2005; Bestmann et al. 2010).

It is, perhaps, surprising to find ÔÔthick" H_nBH_n boundaries in samples annealed for one year (Figs. 5g, 7g). On the other hand, there is no evidence that the few% brine present in the samples after compaction was expelled by a sintering-like process during annealing, so that the brine must have been redistributed in the samples. Considering that some grain boundaries did heal during annealing, the presence of the thick boundaries is interpreted to be a necessary part of the annealing process. Even if there was a potential difference across these boundaries, these ÔÔthickÕÕ H_nBH_n are interpreted to have a very low mobility due to the long diffusion path across the thick grain boundary. (Urai et al. 1986b)

Model for evolution of brine distribution during static recrystallization in coarse-grained halite

In what follows, we attempt to compile our results and interpretations (Fig. 10) in a model for the evolution of brine distribution in wet sodium chloride aggregates during static recrystallization.

From the initial compaction to the complete recovery of samples, steps are as following:

1. The initial compaction of polycrystalline salt plugs produced abundant intracrystalline defects and microcracks favorable to nucleation of strain-free grains at these sites, together with much smaller grains, which were not removed by sieving. (A. in Fig. 10). Primary recrystallization then proceeds in an isotropic stress field of zero effective stress in fully saturated samples under static conditions without intracrystalline recovery processes inside the deformed grains since annealing was performed at room temperature (Schenk and Urai 2004). There are no external forces to increase the normal stress on brine-filled grain boundaries. Euhedral grains grow into deformed grains by brine-assisted grain boundary migration (Fig. 9).
2. Driven by very small, local differences in brine concentration, some deformed grains are interpreted to grow low-index facets (B. in Fig. 10). This ÔÔrimÕÕ of undeformed, faceted halite can locally prevent the migration of a neighbor into this grain but it still needs to be checked using EBSD measurement.
3. Therefore, the evolution of microstructure over time involves three main grain boundary contacts: (1) contact between two old deformed grains (Inset B.1

Fig. 10 Model for evolution of brine distribution during coarsening of chloride sodium aggregate during static recrystallization. *Cation* spheres point to impingement sites in B.4 (in C). See details in text

in C. Fig. 10), (2) contact between an old deformed grain and a grain developing low-index faces (Inset B.2 in Fig. 10), and (3) contact involving two grains developing low-index faces (Insets B.4 and B.5 in Fig. 10).

If the grain boundary involves two old deformed grains with thick brine Þlm (H_nBH_n), the grain boundary has a very low mobility.

If the grain boundary consists of a deformed grain and a new grain with low-index faces, ($H_{fr}BH_b$), and the grain boundary is brine-Þlled (50 nm), the new grain grows into the deformed grain, driven by reduction of dislocation density, and facilitated by the fact that the B_{fr} side of the faceted boundary is irrational (Insets B.2 and B.3 in Fig. 10; Passchier and Trouw 2005; Schenk and Urai 2004; Humphreys and Hatherly 1996).

If the grain boundary involves two grains developing low-index faces ($H_{fr}BH_{fr}$), both crystals continue to grow until they impinge. Our interpretation is that part of the boundary becomes solidÐsolid (HH) (Insets B.4 and B.5 in Fig. 10).

5. Driven by the incipient of grain boundary healing process, brines at impingement evolve as isolated inclusions (C. in Fig. 10): (a) ÔÔelongated-shapedÕÕ IBI appear at interface of two F faces, (b) aligned ÔÔquandrangle-shapedÕÕ IBI are at contact of a S or K face with an other S or K face, and (c) ÔÔtriangle-shapedÕÕ IBI involve one F face with one S or K face. Intragranular big ÔÔquadrangle-shapedÕÕ IBI are leftover brine inclusions behind migrating grain boundary.

Conclusions

- BIB-cryo-SEM allows direct in situ investigations of brine-Þlled grain boundaries in wet halite polycrystals, resolving brine Þlms in grain boundaries down to 15 nm thicknesses.
- Our observations are consistent with earlier work on brine-assisted grain boundary migration in wet halite and provide new information on the evolution of grain boundary structure.
- Brine-Þlled grain boundary migration is strongly affected by the development of facets. These facets can be rational or irrational and lead to migration, impingement, and healing of the grain boundary.
- Grain boundary healing locally produces boundaries in which our instrument cannot resolve brine Þlm. We interpret these to be healed, solidÐsolid boundaries.
- Some brine-Þlled grain boundaries remain several micrometers thick over annealing periods of over a year.

Acknowledgments We thank the Deutsche Forschungsgemeinschaft for supporting our project and funding the BIB-cryo-SEM instrument (Project UR 64/9-2). We are also grateful to Dr. Georg Koschek, Dr. Christian Jaeger and Mr. Hans-Rolf Schreiber from Carl Zeiss NTS GmbH, and Dr. Sebastian van Offern from Klocke Nanotechnik GmbH for their work to help us to develop the BIB-cryo-SEM instrument. We thank Prof. Dr. F. Michael Meyer from Institut für Mineralogie und Lagerstättenlehre at RWTH Aachen University for hosting the instrument; and Franz-Günter from the Geological Institute at RWTH Aachen University for his help with installing the instrument.

References

Beaupêtre S, Zigone D, Voisin C, Renard F (2010) On the healing rate of a reactive interface. EGU2010-8599

Berest P, Brouard B, Karimi-Jafari M (2010) A 12-year cavern abandonment test. In: EPJ Web of Conferences, vol 6, pp 22003Ð22010

Brantley SL, Evans B, Hickman SH, Crerar DA (1990) Healing of microcracks in quartz: implications for ßuid ßow. Geology 18:136

De Meer S, Spiers CJ, Peach CJ, Watanabe T (2002) Diffusive properties of ßuid-Þlled grain boundaries measured electrically during active pressure solution. Earth Planet Sci Lett 200:147Ð157

De Meer S, Spiers C, Nakashima S (2005) Structure and diffusive properties of ßuid-Þlled grain boundaries: an in situ study using infrared (micro) spectroscopy. Earth Planet Sci Lett 232:403Ð414

De Winter AMD, Schneijdenberg C, Lebbink M, Lich B, Verkleij A, Drury M, Humbel B (2009) Tomography of insulating biological and geological materials using focused ion beam (FIB) sectioning and low-kV BSE imaging. J Microsc 233:372Ð383

Den Brok BD, Morel J, Zahid M (2002) In situ experimental study of roughness development at a stressed solid/ßuid interface, vol 200. Geological Society, London, Special Publications, pp 73Ð83. doi:10.1144/GSL.SP.2001.200.01.05

Desbois G, Urai JL, Burkhardt C, Drury MR, Hayles M, Humbel B (2008) Cryogenic vitriÞcation and 3D serial sectioning using high resolution cryo-FIB SEM technology for brine-Þlled grain boundaries in halite: Þrst results. Geoßuids 8:60Ð72

Desbois G, Urai JL, Kukla PA (2009) Morphology of the pore space in claystonesÑevidence from BIB/FIB ion beam sectioning and cryo-SEM observations. eEarth 4:15Ð22

Desbois G, Zavada P, Schleder Z, Urai JL (2010) Deformation and recrystallization mechanisms in naturally deformed salt fountain: microstructural evidence for a switch in deformation mechanisms with increased availability of meteoric water and decreased grain size (Qum Kuh, central Iran). J Struct Geol 32(4):580Ð594

Drury M, Urai J (1990) Deformation-related recrystallization processes. Tectonophysics 172:235Ð253

Fujiwara K, Tsumura S, Tokairin M, Kutsukake K, Usami N, Uda S, Nakajima K (2009) Growth behavior of faceted Si crystals at grain boundary formation. J Cryst Growth 312(1):19Ð23

Ghoussoub J, Leroy YM (2001) SolidÐßuid phase transformation within grain boundaries during compaction by pressure solution. J Mech Phys Solids 49:2385Ð2430

Gratier J (1993) Experimental pressure solution of Halite by an indenter technique. Geophys Res Lett 20:1647

Hartman P, Perdok WG (1955) On the relations between structure and morphology of crystals. I Acta Crystallogr 8:49Ð52

Heidug WK, Leroy YM (1994) Geometrical evolution of stressed and curved solidÐßuid phase boundaries 1. Transformation kinetics. J Geophys Res 99:505Ð515

Hickman SH, Evans B (1991) Experimental pressure solution in halite: the effect of grain/interphase boundary structure. J Geol Soc 148:549Ð560

Hickman SH, Evans B (1995) Kinetics of pressure solution at halite-silica interfaces and intergranular clay Þlms. J Geophys Res 100:13113

Hippert J, Egydio-Silva M (1996) New polygonal grains formed by dissolutionÐredeposition in quartz mylonite. J Struct Geol 18:1345Ð1352

Holness M, Lewis S (1997) The structure of the halite-brine interface inferred from pressure and temperature variations of equilibrium dihedral angles in the halite-H2OÐCO2 system. Geochim Cosmochim Acta 61:795Ð804

Holzer L, Cantoni M (2011) Review of FIB-tomography. In: Utke I, Moshkalev S, Russell Ph (eds) Nanofabrication using focused ion and electron beams: principles and applications. Oxford University Press, NY. ISBN 9780199734214

Holzer L, Gasser P, Kaech A, Wegmann M, Zingg A, Wepf R, Muench B (2007) Cryo-FIB-nanotomography for quantitative analysis of particle structures in cement suspensions. J Microsc 227:216Ð228

Holzer L, Münch B, Rizzi M, Wepf R, Marschall P, Graule T (2010) 3D-microstructure analysis of hydrated bentonite with cryo-stabilized pore water. Appl Clay Sci 47:330Ð342

Hudec M, Jackson M (2007) Terra inÞrma: understanding salt tectonics. Earth-Sci Rev 82:1Ð28

Humphreys J, Hatherly M (1996) Recrystallization and related annealing phenomena, Reprinted with corr. ed. Pergamon, Oxford [u.a.]

Langer M (1993) Use of solution-mined caverns in salt for oil and gas storage and toxic waste disposal in Germany. Eng Geol 35:183Ð190

Lehner F (1995) A model for intergranular pressure solution in open systems. Tectonophysics 245:153Ð170

Littke R, Bayer U, Gajewski D, Nelskamp S (2008) Dynamics of complex intracontinental BasinsÑThe Central European Basin System. Springer, BerlinÐHeidelberg, ISBN: 978-3-540-85084-7

Lohkaemper THK, Jordan G, Costamagna R, Stoeckhert B, Schmahl WW (2003) Phase shift interference microscope study of dissolution-precipitation processes of nonhydrostatically stressed halite crystals in solution. Contrib Mineral Petrol 146:263Ð274

Loucks RG, Reed RM, Ruppel SC, Jarvie DM (2009) Morphology, genesis, and distribution of nanometer-scale pores in siliceous mudstones of the Mississippian Barnett Shale. J Sediment Res 79:848Ð861

Passchier CW, Trouw RAJ (2005) Microtectonics, 2nd edn. Springer, Berlin, New York

Pincus H (1985) Underground storage of oil and gas in salt deposits and other non-hard rocks. Earth-Sci Rev 22:238Ð239

Renard F, Bernard D, Thibault X, Boller E (2004) Synchrotron 3D microtomography of halite aggregates during experimental pressure solution creep and evolution of the permeability. Geophys Res Lett 31:L07607. doi:10.1029/2004GL019605

Schenk O, Urai JL (2004) Microstructural evolution and grain boundary structure during static recrystallization in synthetic polycrystals of Sodium Chloride containing saturated brine. Contrib Mineral Petrol 146:671Ð682

Schenk O, Urai JL (2005) The migration of ßuid-Þlled grain boundaries in recrystallizing synthetic bischoÞte: Þrst results of in situ high-pressure, high-temperature deformation experiments in transmitted light. J Metamorph Geol 23:695Ð709

Schenk O, Urai JL, Piazolo S (2006) Structure of grain boundaries in wet, synthetic polycrystalline, statically recrystallizing haliteÑ evidence from cryo-SEM observations. Geoßuids 6:93Ð104

Schleder Z, Urai JL (2005) Microstructural evolution of deformation-modiÞed primary halite from the Middle Triassic Röt Formation at Hengelo, The Netherlands. Int J Earth Sci (Geol Rundsch) 94:941Ð955

Schmatz J, Schenk O, Urai JL (2010) The interaction of migrating grain boundaries and ßuid inclusions in rock analogues: the effect of wetting angle and ßuid inclusion velocity. Contrib Mineral Petrol. 162(1):193Ð208. doi:10.1007/s00410-010-0590-3

Schoenherr J, Urai J, Kukla PA, Littke R, Schleder Z, Larroque J-M, Newall M, Al-Abry N, Al-Siyabi H, Rawahi Z (2007) Limits to the sealing capacity of rocksalt: a case study of the Infra-Cambrian Ara Salt from the South Oman Salt Basin. AAPG Bull 91(11):1541Ð1557

Spiers CJ, Schutjens PMTM (1999) Intergranular pressure solution in Nacl: grain-to-grain contact experiments under the optical microscope. Oil Gas Sci Technol Rev IFP 54:729Ð750

Spiers CJ, Urai JL, Lister GS, Boland JN, Zwart HJ (1986) The inßuence of ßuid rock interaction on the rheology of salt rock and on ionic transport in the salt. Nuclear Science and Technology EUR 10399 EN, Luxembourg, p 131

Spiers CJ, Brzesowskry RH, Peach CJ, Liezenberg JL, Zwart HJ (1990) Experimental determination of constitutive parameters governing creep of rocksalt by pressure solution. In: Knipe RJ, Ruitter EH (eds) Deformation mechanisms, rheology, and tectonics, vol 54. Geological Society, London, Special Publication, pp 215Ð227. doi:10.1144/GSL.SP.1990.054.01.21

Staudtmeister K, Rokahr R (1997) Rock mechanical design of storage caverns for natural gas in rock salt mass. Int J Rock Mech Min Sci 34:300.e1Ð300.e13

Urai JL, Means WD, Lister GS (1986a) Dynamic recrystallization of minerals. In: Hobbs, B. E., Heard, H. C. (Eds.), Mineral and Rock Deformation: Laboratory Studies - The Paterson Volume. American Geophysical Union, Geophysical Monograph 36:161Ð199

Urai JL, Spiers CJ, Zwart HJ, Lister GS (1986b) Weakening of rock salt by water during long-term creep. Nature 324:554Ð557

Urai JL, Schleder Z, Spiers C, Kukla PA (2008) Flow and transport properties of salt rocks. In: Littke R, Bayer U, Gajewski D, Nelskamp S (eds) Dynamics of complex intracontinental basins: The Central European Basin System. Springer, Berlin, Heidelberg 277-290.978-3-540-85084-7

Van Noort R, Spiers CJ, Peach CJ (2006) Effects of orientation on the diffusive properties of ßuid-Þlled grain boundaries during pressure solution. Phys Chem Miner 34:95Ð112

Van Noort R, Visser HJM, Spiers CJ (2008) Inßuence of grain boundary structure on dissolution controlled pressure solution and retarding effects of grain boundary healing. J Geophys Res 113:B03201. doi:10.1029/2007JB005223

Visser HJM (1999) Mass transfer processes in crystalline aggregates containing a ßuid phase. PhD thesis, Universiteit Utrecht, 244 pp

Watanabe T, Peach CJ (2002) Electrical impedance measurement of plastically deforming halite rocks at 125 and 50 MPa. J Geophys Res (Solid Earth) 107:B1. doi:10.1029/2001JB000204